Contract No.:

This manuscript has been authored by Savannah River Nuclear Solutions (SRNS), LLC under Contract No. DE-AC09-08SR22470 with the U.S. Department of Energy (DOE) Office of Environmental Management (EM).

Removal capacity and chemical speciation of groundwater iodide (I^-) and iodate (IO_3^-) sequestered by organoclays and granular activated carbon

Dien Li[a,*], Daniel I. Kaplan[a], Allison Sams[b], and Brian A. Powell[b] , Anna S. Knox[a]

[a] Savannah River National Laboratory, Aiken, SC 29808, USA

[b] Department of Environmental Engineering and Earth Sciences, Clemson University, Anderson, SC 29625, USA

[*] Corresponding author.

Email: Dien.Li@srs.gov. (D. Li).

ABSTRACT: Radioiodine (I) is difficult to remove from aqueous waste streams or contaminated groundwater because of its tendency to exist as multiple anionic species in the same system (i.e., iodide (I^-), iodate (IO_3^-) and organo-iodide) that tend not to bind to minerals or synthetic materials. In this work, the efficacy of organoclays and granular activated carbon (GAC) to bind I^- and IO_3^- from artificial groundwater (AGW) was tested. The organoclays and GAC were highly effective at removing I^- and IO_3^- from AGW under oxic condition. The adsorption capacities of I^- and IO_3^- on the organoclays and GAC were up to 30 mg I/g sorbent. While the I^- adsorption behavior was well described by Langmuir model, the IO_3^- adsorption behavior was better described by the Freundlich model. Based on XANES measurements, I^- and IO_3^- species were likely bound with N ligands on the organoclay and GAC surface through electrostatic attraction, but with two exceptions. First, when GAC was exposed to I^- in

groundwater, the sequestered I species was molecular I_2. Second, I species on one of the organoclay samples (OCM) exposed to IO_3^- became I^- likely bound with organic ligands, rather than IO_3^-. Thus, the inexpensive and high-capacity organoclays and GAC may provide a practical solution of removing ^{129}I contaminant from environmental systems and liquid nuclear wastes.

Keywords: Iodide, Iodate, Organoclays, Granular activated carbon, Synchrotron XANES and EXAFS

1. Introduction

^{129}I is a major long-lived fission product generated during nuclear power production. Over the years, I contaminant species have been inadvertently introduced into the environment from leaks at waste storage facilities and currently are key risk drivers at several US DOE sites [1]. The most common chemical forms of I in liquid nuclear wastes and in the environment are anionic iodide (I^-), iodate (IO_3^-), and organo-iodine, and these I species very often co-exist in the environmental systems [1]. They display limited adsorption onto common sediment minerals or even expensive synthetic materials, making them highly mobile and difficult to remove from the aqueous phase. As the stockpile of ^{129}I-bearing nuclear waste continues to increase rapidly due to nuclear energy production, novel and practical sequestration technologies are needed to reduce its potential contamination of the environment and living organisms.

Different minerals (e.g., metal sulfides, hydrotalcites and silicates) [2-5], organoclays [6-9], natural organic material [10-12], metal oxides [13], composite absorbents [14], activated carbon [15] and nanomaterials [16] have been tested for iodine removal from liquid phases. The most effective materials for iodine removal are silver chloride [14, 17], argentite (AgS) [18], and Ag modified activated carbon, zeolites and porous silica [16, 18-27], presumably to form insoluble

AgI. However, the Ag-based materials are only effective for removing iodide (I^-) and maybe organo-iodine [3, 27-29], but not iodate (IO_3^-). A recent study demonstrated that IO_3^- can be immobilized into calcium carbonate by synchrotron X-ray absorption spectroscopy and first-principle calculation [30]. In addition, IO_3^- has been demonstrated to substitute for CO_3^{2-} in $Na_4UO_2(CO_3)_3$ [31] and aragonite [32].

In our previous work, organoclays and GAC were demonstrated to display high adsorption coefficients (K_d) for removing TcO_4^-, I^- and Cs^- from AGW under oxic conditions [33]. The adsorption capacities for TcO_4^- removal from AGW under varying pH conditions were further determined to be as high as 15 mg/g for organoclays and 25 mg/g for GAC under oxic conditions. The chemical speciation of Tc on the organoclays and GAS remained TcO_4^-, rather than converting to its less soluble and reduced form of Tc(IV) [34]. For this study, we extended our study of these sorbents to quantify and understand the binding processes with aqueous I^- and IO_3^-. The objectives of this work were: 1) quantify the adsorption capacities of the organoclays and GAC for removing I^- and IO_3^- from AGW under oxic conditions using batch adsorption experiments, with particular attention to evaluating the effects on this process of NO_3^- competition, and 2) identify I chemical speciation on the organoclays and GAC using I K-edge X-ray absorption near structure (XANES) and extended X-ray absorption fine structure (EXAFS).

2. Materials and methods

2.1 Materials

Organoclay OCB was purchased from Biomin Inc. (Ferndale, MI). It is composed of a bentonite clay and an impregnated quaternary amine flocculant. Organoclay OCM was

purchased from Cetco® Remediation Technologies (Hoffman Estates, IL). A bentonite clay was impregnated with a quaternary amine and the organoclay was intimately mixed with a sulfur-containing compound [35]. The GAC material used in this study was purchased from Norit America, Inc. (Marshall, TX). The GAC was made from a coal of selected grade using high temperature steaming activation. In addition, potassium iodide (KI), potassium iodate (KIO_3) and sodium nitrate ($NaNO_3$) were purchased from Fisher Scientific, while 4-iodoaniline (C_6H_6IN) was from Thermofisher Acros Organics (Geel, Belgium). The chemicals were used as received. The certain amount of each of KI and KIO_3 was dissolved in artificial groundwater to prepare iodide (5×10^{-3} M) and iodate (5×10^{-3} M) stock solutions that were used for batch sorption experiments. The artificial groundwater (AGW) solution is a simulant of a typical uncontaminated groundwater from the Savannah River Sites [36]. The chemical composition (in mg/L) of AGW was Na 1.25, K 0.25, Ca 0.93, Mg 0.66, Cl 5.51, and SO_4 0.73. It had a pH ~6.3, an electrical conductivity of 0.03 mS/cm, and a turbidity of 4.1 NTU [37].

2.2 Batch sorption experiments

Batch sorption experiments for obtaining the adsorption isotherms (the mass (q_e, mg/g) on the sorbent versus the concentration in solution at equilibrium) were conducted in AGW under ambient atmosphere and temperature (22 °C). For each set of experiments, a sorbent-free control was included as the initial I concentration for q_e calculation and to provide an indication of I sorption to the labware during the experiment. 0.05-5 mL of the I (i.e., I^- or IO_3^-) stock solution (5×10^{-3} M) was spiked to make the final working solution of 5 mL in the I concentrations ranging from 5×10^{-5} M to 5×10^{-3} M. Background levels for stable iodine are commonly in the micromolar range and contaminant groundwater ^{129}I concentration generally do not exceed 0.1 µM [1], but more elevated concentrations were used in this study to ease analytical

91 measurements with these strong sorbents and to permit detection by synchrotron XANES and
92 EXAFS. The sorbent concentration was 0.05 g/5 mL or 1 %. The suspensions were shaken on a
93 reciprocating shaker for 6 days. After equilibrium, the pH levels of the suspensions were
94 measured (Radiometer Copenhagen PHM 95 pH meter) and each suspension was filtered using a
95 0.2 μm pore size nylon membrane filter. The filtrate was analyzed for I by inductively coupled
96 plasma mass spectrometry (ICP-MS; Thermo XSeries II ICP-MS). The ICP-MS analyses had an
97 uncertainty of ± 10%, but our repeatability test indicated that this uncertainty was often within ±
98 5%. The solid samples were air dried and some of them were selected for spectroscopic
99 characterization. To evaluate the effects of competitive NO_3^- on I^- and IO_3^- removal capacities of
100 the organoclays and GAC, batch experiments were conducted using 0.05 g sorbents and 5 mL of
101 AGW with or without extra 0.1 M $NaNO_3$ at the initial concentrations of 3×10^{-3} M for I^- or IO_3^-.

102 *2.3 I K-edge XANES and EXAFS*

103 After batch adsorption experiments, I K-edge XANES and EXAFS spectra of selected
104 organoclays and GAC samples were collected using the Materials Research Collaborative
105 Access Team (MRCAT) Sector 10-BM beamline at the Advanced Photon Source (APS)
106 (Argonne National Lab, Argonne, IL). To do so, 50 mg of each of the air-dried powder samples
107 was pressed into a 6.3-mm diameter disk pellet that was mounted on sample holder. The
108 MRCAT Sector 10-BM beamline used a double crystal water cooled Si (111) monochromator,
109 detuned to 50% of peak intensity [38]. The monochromators were calibrated using the first
110 inflection point at 31,814 eV of the K-edge of tellurium foil. The I K-edge XANES and EXAFS
111 spectra were taken in transmission mode in the energy range of 33,000-34,000 eV at room
112 temperature.

Spectra were processed and analyzed using the IFEFFIT software package including Athena and Artemis [39]. Data from multiple scans were processed using Athena by aligning and merging the spectra followed by background subtraction using the AUTOBK algorithm. I K-edge EXAFS data analysis was conducted on the merged and normalized spectra using Artemis. Crystalline I_2 was used as a reference structural model [40] for EXAFS data fitting of GAC 830 exposed to iodide. Fits to the I EXAFS data were made in R space (R from 1 to 4.3 Å) and obtained by taking the Fourier transform (FT) of $\chi(k)$ (k from 1.8 to 6.8) with a k weighting of 2, because the $\chi(k)$ spectra above k = 6.8 very noisy, which caused the artifact feature around 1 Å in the Fourier transforms of $\chi(k)$ spectra.

3. Results and discussion

3.1 Capacities of organoclays and GAC for iodide (I^-) removal

From the batch experiments, the mass of I^- sorbed onto the sorbent (q_e, mg/g) were calculated using equations 1:

$$q_e = \frac{(C_0 - C_e) \times V}{M} \quad (1)$$

where C_0 (mg/L) is the initial I^- concentration in the control samples, C_e (mg/L) is I concentration in the solution at equilibrium, V is the volume of the solution (mL) and M is the mass of the sorbent (g). The adsorption isotherms of I^- onto organoclay OCB, organoclay OCM and GAC 830 in AGW under oxic condition are shown in Fig. 1. The I^- adsorption isotherms for organoclays OCB and OCM and GAC 830 appear to approach the sorption plateaus indicative of sorbent saturation capacity. The air-dried sorbent samples after iodide adsorption selected for spectroscopic measurements were labelled.

These isotherm data were fitted using the Langmuir isotherm model (equation 2). The Langmuir model assumes that adsorption occurs as a monolayer on an energetically homogeneous surface without interaction between the adsorbates on adjacent sites:

$$\frac{C_e}{q_e} = \frac{1}{q_{\max}} C_e + \frac{1}{K_L \times q_{\max}} \qquad (2)$$

where q_e is the mass of I^- sorbed onto the sorbent at equilibrium, q_{max} is the saturation sorption capacity, C_e is the I^- concentration in solution at equilibrium, and K_L is the Langmuir constant that is directly related to the binding site affinity. The Langmuir fits to the corresponding experimental data are shown in the inset of Fig. 1. The I^- saturation adsorption capacities of organoclays OCB and OCM and GAC 830, together with R^2 that measures the fitting quality, are presented in Table 1. The adsorption isotherms for the organoclays OCB and OCM and GAC 830 were well fitted to Langmuir model, as indicated by R^2 numbers. The saturation capacity for iodide removal from AGW was 21.1 mg/g for organoclay OCB at the equilibrium pH of 12.1, 27.5 mg/g for organoclay OCM at the equilibrium pH of 8.0 and 29.9 mg/g for GAC 830 at the equilibrium pH of 7.9. These are comparable with the reported sorption capacity (~0.5 mol/kg or ~64 mg/g) of hexadecylpyridinium functionalized bentonite for I^- removal from different equilibrium solutions [6].

3.2. Capacities of organoclays and GAC for iodate (IO_3^-) removal

Similarly, the adsorption isotherms of OCB, OCM and GAC 830 for iodate removal from AGW are shown in Fig. 2. The profiles of iodate adsorption isotherms increased gradually and looked more like a linear behavior, and the iodate saturation plateau indicative of saturated capacities for all three sorbents were not realized. The Freundlich model (equation 3) better fit the experimental isotherm data, as shown in the inset of Fig. 2, rather than by Langmuir model:

$$\ln(q_e) = \ln(k_f) + (\frac{1}{n}) \times \ln(C_e) \qquad (3)$$

where C_e and q_e are defined as in the Langmuir isotherm (i.e., equation 2), k_f (L/g) and n are the Freundlich constants relating to sorption capacity and sorption intensity, respectively. The Freundlich constants for the iodate sorption on organoclays and GAC 830 in AGW are also shown in Table 1. Although the saturation capacities of the three sorbents for iodate removal might not be quantitatively determined, Fig. 2 shows that the removal capacity of OCB, OCM and GAC 803 for iodate from AGW was equivalent to or even greater than the corresponding capacity for iodide removal. In addition, for OCB and GAC 830, the Freundlich constant k_f (L/g) for iodate removal was reasonably similar to the corresponding Langmuir constant K_L (L/g) for iodide removal. The iodate (IO_3^-) could form outer sphere complexation with the binding sites, saying N ligands on organoclays or similar surface ligands on GAC 830.

3.3. Effect of competitive NO_3^- on removal capacities

Competitive anions (e.g., NO_3^-, HCO_3^-, SO_4^{2-} and PO_4^{3-}) are commonly present in contaminated environments and can compromise the capability of the organoclays and GAC sorbents for removing aqueous I^- and IO_3^-. In order to evaluate the effects of competitive NO_3^- on I^- and IO_3^- removal capacities, batch experiments were conducted using 0.05 g sorbents and 5 mL of AGW with or without extra 0.1 M $NaNO_3$ at the initial concentrations of 3×10^{-3} M for both I^- and IO_3^-. The results are shown in Fig. 3, which demonstrated that additional 0.1 M $NaNO_3$ into AGW in general decreased the capacities of all three sorbents for removing I^- and IO_3^- by 10-50%. However, it is unclear why the IO_3^- removal capacity of organoclay OCB was higher from AGW in presence of 0.1 M $NaNO_3$ than from AGW without 0.1 M $NaNO_3$, probably due to experimental and/or analytical errors. Because NO_3^- was nearly two orders of

179 magnitude greater than the I concentrations in the AGW containing 0.1 M $NaNO_3$, the results
180 demonstrated that the organoclay and GAC sorbents show reasonably good selectivity toward I^-
181 and IO_3^- over NO_3^-. However, considering that ^{129}I contaminant concentration levels are 10^{-7} M,
182 whereas background nitrate levels are often 10^{-3} M, in systems (e.g., engineered waste streams)
183 where very high NO_3^- concentrations are expected, reduced organoclay and GAC efficiency
184 should be expected.

185 *3.4. I speciation on organoclays and GAC after exposed to I^-*

186 After the adsorption batch experiments, two air-dried sorbent samples for each of the
187 organoclays OCB, OCM and GAC 830 were selected for I K-edge XANES and EXAFS
188 measurements in order to determine I chemical speciation on the sorbent materials. The I K-edge
189 XANES (A), EXAFS spectra in k-space (B) and Fourier transforms in magnitude (C) of the air-
190 dried sorbents are shown in Fig. 4, in which the corresponding spectra of I_2, KI, and 4-
191 iodoaniline are included for comparison. The equilibrium pH levels in these batch experiments
192 were 12.28 ± 0.05 for organoclay OCB, 7.92 ± 0.04 for organoclay OCM and 8.25 ± 0.08 for
193 GAC 830. The sample identifications were labeled in the adsorption isotherm graphs for iodide
194 (I^-) on organoclays and GAC 830 in AGW (Fig. 1.)

195 The I K-edge XANES spectra of the standards are similar to those reported in literature [12,
196 41-44]. Due to shorter core–hole lifetimes during X-ray absorption processes for higher atomic
197 number elements like I, the I K-edge XANES features are broadened. As a result, it is difficult to
198 distinguish clear I K-edge energy shifts between iodide and I_2 standard samples. While there is a
199 relatively identifiable peak after the absorption edge of KI, the 4-iodoaniline and I_2 have nearly
200 featureless XANES with weak oscillation amplitude at energies higher than the absorption edge.
201 The I K-edge XANES spectra (Fig. 4A) of organoclays OCB and OCM and GAC 830 exposed

to iodide are nearly featureless at energies above the absorption edge that is also shown little energy shift among these samples, which are similar to the XANES spectra of 4-iodoaniline and I_2. However, the I K-edge XANES spectra alone appears not able to exclusively determine the I species (e.g., organoiodine species or molecular I_2) on the organoclays and GAC, but the corresponding EXAFS data that will be discussed below can provide more distinctive identification of these iodine species.

The $\chi(k)$ EXAFS spectra (Fig. 4B) and their corresponding Fourier transforms in magnitude (Fig. 4C) of organoclays OCB and OCM were similar. There were two distinctive oscillation features at k = 3-5, but the spectra were noisy and featureless above k = 5. The Fourier transforms in magnitude of the organoclays OCB and OCM show a broad peak between R = 2-3 Å, but it is uncertain if the weak peak around 1 Å was real or an artifact due to noise data at k > 5. Because there were limited oscillations in the EXAFS data, the EXAFS data fitting to obtain more quantitative information was unsuccessful. However, the two oscillation features of organoclay OCB and OCM that sequestered iodide are qualitatively similar to the two oscillation peaks of 4-iodoaniline around k = 4, which may indicate that iodine chemical species on the organoclays were like organo-iodine. Iodide (I^-) was bound with organic quaternary amines in the organoclays likely through the electrostatic attraction between I^- and N ligands. On the other hand, the $\chi(k)$ EXAFS spectra (Fig. 4B) and corresponding Fourier transform in magnitude (Fig. 4C) of GAC samples exposed to I^- were significantly different from those of organoclays with I^- adsorption and 4-iodoaniline, but visibly similar to the $\chi(k)$ spectrum (Fig. 4B) and Fourier transform in magnitude of I_2.

In order to understand iodine chemical speciation on GAC further, the EXAFS data of two GAC samples and standard I_2 were fitted by using molecular I_2 as a structure model [40]. I K-

edge EXAFS spectra in k-space (A), Fourier transforms plots in magnitude (B) and in the real space component (C) of the two GAC 830 samples after exposed to I^- in the AGW and standard I_2 are shown in Fig. 5, where experimental data are shown in solid circles, and EXAFS fits are shown in color lines. The fitted EXAFS parameters of the two GAC samples and standard I_2 are summarized in Table 2. The EXAFS spectrum of I_2 was fitted by the first I-I path with I-I distance of 2.703 Å and fixed coordination number of 1 and the second I-I path with I-I distance of 3.538 Å and fixed coordination number of 2. The EXAFS fitting of this model compound was good as measured by reduced χ^2 of 1.22 and R-factor of 0.0034. The obtained first I-I distance was slightly longer (2.837 Å) than X-ray diffraction I-I distance of 2.703 Å, while the second I-I distance was unexpectedly shorter (3.309 Å) than that X-ray diffraction data (3.538 Å). The Debye–Waller factor, σ^2, is large, 0.0179 $Å^2$ for the first I-I path and 0.0773 $Å^2$ for the second I-I path, but they were not unusual compared to literature in which σ^2 was reported for the first I-I path at 0.0167 $Å^2$ and for the I-K path of KI at 0.0223 $Å^2$ [41]. The EXAFS data of the two GAC samples were fitted well using I_2 structure model with the R-factor of 0.0281 and 0.0102, respectively. The addition of the third I-I path at ~4.348 Å slightly improved the fitting statistics. The obtained I-I bond distance for each path was similar to the corresponding X-ray diffraction bond distance, and the obtained Debye–Waller factor, σ^2, for each path was also similar to that of the standard I_2 in this work, as well as of NaI, KI and CaI_2 reported in literature [41]. The results demonstrated that the chemical speciation of iodine on granular activated carbon exposed to iodide in artificial groundwater is likely molecular I_2.

The interaction of doped iodine specie with hosting carbon materials was investigated [45-50]. As iodine is intercalated into carbon single wall nanotubes (SWNBs), the speciation of charged polyiodide chains (I_n^-) has been identified [46], even though it is controversial about the

intercalation sites and structure of iodine. It has been suggested that I_n^- molecules might reside both in the interstitial channels and inside the tubes of SWNTs bundles [48] or mainly inside the tubes [49]. Iodine atoms were also revealed to incorporate in the form of helical chains inside the SWNTs, but substantial iodine species are also incorporated in the interstitial position between tubes in the bundles [45]. More recent I K-edge EXAFS data indicated that iodine chain species enter inside SWNTs as disordered pentaiodide (I_5^-) [50]. The iodine species I_n^- is also identified in iodine-doped carbon multiple wall nanotubes (MWNTs) [47], and the iodine-carbon host interaction is weaker in MWNTs than in carbon SWNTs, and the I_n^- species are only localized at the surface of the external tube for MWNTs [50]. The spacing between graphene sheets in graphite cannot accommodate iodine species [51]. In our case of granular activated carbon exposed to iodide in artificial groundwater, the I_2 or I_n^- chain species were identified through the I K-edge EAXFS data. However, the I-C scattering path could not be exclusively identified because noisy data at $k > 6$ caused artifact features at $R < 2$ Å after Fourier transform. Thus, in agreement with previous studies, the iodine species sequestered on GAC was likely molecular I_2 or I_n^- chain species that was adsorbed on the external surfaces of GAC.

3.5. I speciation on organoclays and GAC after exposed to IO_3^-

Similarly, the I K-edge XANES (A), EXAFS spectra in k-space (B) and Fourier transforms in magnitude (C) of the air-dried sorbents after exposed to iodate (IO_3^-) in AGW are shown in Fig. 6. The corresponding spectra of KIO_3 and 4-iodoaniline are included for comparison. These sorbent samples were collected from the batch experiment in which the equilibrium pH levels were 12.44 ± 0.02 for organoclay OCB, 7.25 ± 0.07 for organoclay OCM and 7.77 ± 0.09 for GAC 830. The sample identifications were labeled in the adsorption isotherm graphs for iodate (IO_3^-) on organoclays and GAC 830 in AGW (Fig. 2.)

The I K-edge XANES (A), EXAFS spectra in k-space (B) and Fourier transforms in magnitude (C) of organoclay OCB and GAC 830 exposed to iodate in AGW were nearly identical to the corresponding spectra of standard KIO_3. There are two peaks, an edge peak near 33,183 eV and another broader peak near 33,198 eV, in agreement with I K-edge XANES data for iodate reported in literature [12, 41-43]. In addition, relatively large interference oscillations extend well beyond the XANES energy range, as shown in the EXAFS spectra in k space (Fig. 6B). After Fourier transform, there is a well-defined peak between R = 1-2 (Fig. 6C), responding to I-O scattering path [41]. The EXAFS data fitting was conducted for organoclay OCB and KIO_3 exposed to iodate using k from 2-10 and R from 1 to 3 and X-ray diffraction data of KIO_3 [52]. The obtained parameters for the organoclay OCB were I-O bond distance of 1.806 ± 0.006 Å, coordination number of 2.9 ± 0.2, Debye–Waller factor of 0.0009 ± 0.0009 $Å^{-1}$, with the R-factor of 0.0061. In comparison for KIO_3, the corresponding parameters were I-O bond distance of 1.810 ± 0.007 Å, coordination number of 2.7 ± 0.2, and Debye–Waller factor of 0.0009 ± 0.0011 $Å^2$, with the R-factor of 0.0067. The EXAFS spectra of GAC 830 exposed to iodate were also fitted using the same model, with similar fitted parameters, but the fitting statistics was slight poorer. Therefore, both I K-edge XANES and EXAFS data demonstrated that the chemical speciation of iodine on organoclay OCB and GAC 830 after exposed to iodate in AGW remained being iodate (IO_3^-), it may be adsorbed on the sorbent surfaces as an out sphere complex species, as indicated by the absence of the second scattering path beyond the I-O path in the EXAFS data fitting.

In contrast, the I K-edge XANES spectra of two organoclay OCM samples exposed to iodate were featureless at energies above the absorption edge (Fig. 6A), which are similar to the XANES spectrum of 4-iodoaniline. The EXAFS data (Fig. 6B and 6C) of the organoclay OCM

with iodate adsorption were nearly identical to those of organoclays OCB and OCM exposed to iodide in AGW (Fig. 4B and 4C). These results demonstrated that the chemical speciation of iodine on organoclay OCM was iodide that is likely bound with the intercalated organic molecules, even though it was exposed to iodate initially. It is noted that the organoclay OCM was prepared by impregnating a bentonite clay with a quaternary amine first, and then the resulting organoclay was intimately mixed with a sulfur-containing compound [35]. As the organoclay OCM was exposed to iodate in artificial groundwater, iodate was reduced to iodide that was then bound on the intercalated quaternary amine. The possible reaction pathways are as follows:

$$S^0 + O_2 \rightarrow SO_2\ (aq) \quad (4)$$

$$2IO_3^-\ (aq) + 5SO_2\ (aq) + 4H_2O \rightarrow I_2\ (aq) + 8H^+\ (aq) + 5SO_4^{2-}\ (aq) \quad (5)$$

$$I_2\ (aq) + SO_2\ (aq) + 2H_2O \rightarrow 2I^-\ (aq) + 4H^+\ (aq) + SO_4^{2-}\ (aq) \quad (6)$$

These redox reactions were similarly demonstrated by the re-oxidation of reduced low molecular weight subunits of glutenin with KIO_3. Sulfur K-edge XANES spectroscopy shows that reduced low molecular weight subunits of glutenin was re-oxidized by KIO_3 to form disulfide and higher oxidation state sulfur species (e.g., sulfoxide, sulfonic acid) [53].

4. Conclusions

The organoclays and granular activated carbon we studied are very effective in removing iodide (I^-) and iodate (IO_3^-) from groundwater. Under oxic conditions, the adsorption capacity of I^- and IO_3^- on the organoclays and GAC from groundwater were up to 30 mg I/g sorbent. The organoclays and granular activated carbon were demonstrated to be selective for binding I^- and IO_3^- when the competitive anions like NO_3^- are present in the groundwater. The removal capacity

of I contaminant species was mostly reduced by <30% when the NO_3^- concentration in groundwater was nearly two orders of magnitude greater than I^- and IO_3^-. I^- and IO_3^- species are likely bound with N ligands on the organoclay and GAC surface through electrostatic attraction. However, when GAC was exposed to I^- in groundwater, the sequestered I species was I_2 or I_n^- chain species; on the other hand, as organoclay OCM was exposed to IO_3^- in groundwater, IO_3^- was reduced to I^- that is likely bound with the intercalated organic molecules.

For practical applications, silver-based technologies (e.g., AgCl, AgS, and Ag modified activated carbon, zeolites and porous silica) are most successful and commonly applied to remediate iodide from contaminated sites and liquid nuclear wastes, presumably by forming scarcely soluble AgI. However, these technologies are not effective for iodate removal. There are proposals of using a two-step method for removing iodate: first, to reduce iodate to iodide, second, to capture iodide by using a Ag-based material. However, our data demonstrated that organoclay OCM can reduce iodate to iodide and then bind iodide to the interacted organic molecules in a single step. Thus, the inexpensive and high-capacity organoclays and GAC may provide a practical solution of removing ^{129}I contaminant from environmental systems and liquid nuclear wastes.

Acknowledgements

This work was supported by the Laboratory Directed Research and Development (LDRD) program (Grant Nos.: LDRD-2014-00028 and LDRD-2015-00014) within the Savannah River National Laboratory (SRNL). Work was conducted at SRNL under the U.S. Department of Energy Contract DE-AC09-96SR18500. Work conducted at Clemson University was supported by the U.S. Department of Energy Office of Science, Office of Basic Energy Sciences and Office

of Biological and Environmental Research under Award Number DE-SC-00012530.This research used resources (Sector 10) of the Advanced Photon Source, an Office of Science User Facility operated for the U.S. Department of Energy (DOE) Office of Science by Argonne National Laboratory under Contract No. DE-AC02-06CH11357. The MRCAT (Sector 10) operations were also supported by the MRCAT member institutions. We acknowledge Mr. Joshua Wright at the MRCAT for technical assistance during the measurement, and Dr. David McKeown at Vitreous State Laboratory, The Catholic University of America, for the provision of I_2 data.

Bibliography

[1] D.I. Kaplan, M.E. Denham, S. Zhang, C. Yeager, C. Xu, K.A. Schwehr, H.P. Li, Y.F. Ho, D. Wellman, P.H. Santschi, Radioiodine biogeochemistry and prevalence in groundwater, Critical Reviews in Environmental Science and Technology, 44 (2014) 2287-2335.
[2] Y. Ikeda, M. Sazarashi, M. Tsuji, R. Seki, H. Yoshikawa, Adsorption of I- ion on cinnabar form I-129 waste management, Radiochimica Acta, 65 (1994) 195-198.
[3] S.V. Mattigod, R.J. Serne, G.E. Fryxell, Selection and Testing of "Getters" for Adsorption of Iodine-129 and Technetium-99: A Review PNNL-14208, Pacific Northwest National Laboratory, Richland, Washington, 2003.
[4] H. Faghihian, M.G. Maragheh, A. Malekpour, Adsorption of radioactive iodide by natural zeolites, Journal of Radioanalytical and Nuclear Chemistry, 254 (2002) 545-550.
[5] F.L. Theiss, G.A. Ayoko, R.L. Frost, Leaching of iodide (I-) and iodate (IO3-) anions from synthetic layered double hydroxide materials, Journal of Colloid and Interface Science, 478 (2016) 311-315.
[6] J. Bors, S. Dultz, B. Riebe, Organophilic bentonites as adsorbents for radionuclides I. Adsorption of ionic fission products, Applied Clay Science, 16 (2000) 1-13.
[7] J. Bors, Sorption of radioiodine in organo-clays and organo-soils, Radiochimica Acta, 51 (1990) 139-143.
[8] J. Bors, S. Dultz, A. Gorny, Sorption of iodide, cesium and strontium on organophilic bentonite, Radiochimica Acta, 82 (1998) 269-274.
[9] J. Bors, A. Gorny, S. Dultz, Some factors attecting the interactions of organophilic clay-minerals with radioiodine, Radiochimica Acta, 66-7 (1994) 309-313.
[10] S.M. Steinberg, G.T. Schmett, G. Kimble, D.W. Emerson, M.F. Turner, M. Rudin, Immobilization of fission iodine by reaction with insoluble natural organic matter, Journal of Radioanalytical and Nuclear Chemistry, 277 (2008) 175-183.
[11] C. Xu, S. Zhang, Y. Sugiyama, N. Ohte, Y.F. Ho, N. Fujitake, D.I. Kaplan, C.M. Yeager, K. Schwehr, P.H. Santschi, Role of natural organic matter on iodine and (PU)-P-239,240 distribution and mobility in

environmental samples from the northwestern Fukushima Prefecture, Japan, Journal of Environmental Radioactivity, 153 (2016) 156-166.
[12] N. Yamaguchi, M. Nakano, R. Takamatsu, H. Tanida, Inorganic iodine incorporation into soil organic matter: evidence from iodine K-edge X-ray absorption near-edge structure, Journal of Environmental Radioactivity, 101 (2010) 451-457.
[13] X. Zhang, S. Stewart, D.W. Shoesmith, J.C. Wren, Interaction of aqueous iodine species with Ag2O/Ag surfaces, Journal of the Electrochemical Society, 154 (2007) F70-F76.
[14] H. Zhang, X. Gao, T. Guo, Q. Li, H. Liu, X. Ye, M. Guo, Z. Wu, Adsorption of iodide ions on a calcium alginate-silver chloride composite adsorbent, Colloids and Surfaces a-Physicochemical and Engineering Aspects, 386 (2011) 166-171.
[15] P.K. Sinha, K.B. Lal, J. Ahmed, Removal of radioiodine from liquid effluents, Waste Management, 17 (1997) 33-37.
[16] N. Mnasri, C. Charnay, L.-C. de Menorval, Y. Moussaoui, E. Elaloui, J. Zajac, Silver nanoparticle-containing submicron-in-size mesoporous silica-based systems for iodine entrapment and immobilization from gas phase, Microporous and Mesoporous Materials, 196 (2014) 305-313.
[17] M. Denham, M. Millings, J. Noonkester, Post-injection Assessment of the Silver Chloride Field Demonstration for Treatment of I-129 in groundwater at the F-area Seepage Basins, SRNL-TR-2010-00367, Savannah River National Laboratory, Aiekn, SC, 2010.
[18] R.M. Asmussen, J.J. Neeway, A.R. Lawter, A. Wilson, N.P. Qafoku, Silver-based getters for I-129 removal from low-activity waste, Radiochimica Acta, 104 (2016) 905-913.
[19] K.W. Chapman, P.J. Chupas, T.M. Nenoff, Radioactive iodine capture in silver-containing mordenites through nanoscale silver iodide formation, Journal of the American Chemical Society, 132 (2010) 8897-+.
[20] J.S. Hoskins, T. Karanfil, Removal and sequestration of iodide using silver-impregnated activated carbon, Environmental Science & Technology, 36 (2002) 784-789.
[21] S.V. Mattigod, G.E. Fryxell, R.J. Serne, K.E. Parker, Evaluation of novel getters for adsorption of radioiodine from groundwater and waste glass leachates, Radiochimica Acta, 91 (2003) 539-545.
[22] H. Wu, Y. Wu, Z. Chen, Y.Z. Wei, Adsorption behaviors of iodide anion on silver loaded macroporous silicas, Nuclear Science and Techniques, 26 (2015).
[23] M. Kikuchi, M. Kitamura, H. Yusa, S. Horiuchi, Rremoval of radioactive methy iodide by silver impregnated alumina and zeolite, Nuclear Engineering and Design, 47 (1978) 283-287.
[24] S. Sadasivam, S.M. Rao, Characterization of silver-kaolinite (AgK): an adsorbent for long-lived I-129 species, Springerplus, 5 (2016).
[25] G.P. Sheppard, J.A. Hriljac, E.R. Maddrell, N.C. Hyatt, Silver zeolites: iodide occlusion and conversion to sodalite – a potential ^{129}I waste form?, MRS Proceedings, 932 (2006).
[26] M. Sanchez-Polo, J. Rivera-Utrilla, E. Salhi, U. von Gunten, Removal of bromide and iodide anions from drinking water by silver-activated carbon aerogels, Journal of Colloid and Interface Science, 300 (2006) 437-441.
[27] T.M. Nenoff, M.A. Rodriguez, N.R. Soelberg, K.W. Chapman, Silver-mordenite for radiologic gas capture from complex streams: Dual catalytic CH3I decomposition and I confinement, Microporous and Mesoporous Materials, 200 (2014) 297-303.
[28] M. Chebbi, B. Azambre, L. Cantrel, A. Koch, A combined DRIFTS and DR-UV-Vis spectroscopic in situ study on the trapping of CH3I by silver-exchanged faujasite zeolite, Journal of Physical Chemistry C, 120 (2016) 18694-18706.
[29] N.P. Qafoku, J.J. Neeway, A.R. Lawter, T.G. Levitskaia, R.J. Serne, J.H. Westsik, M.M. Valenta Snyder, Technetium and Iodine Getters to Improve Cast Stone Performance PNNL-23282, Pacific Northwest National Laboratory, Richland, Washington, 2014.

[30] J. Podder, J. Lin, W. Sun, S.M. Botis, J. Tse, N. Chen, Y. Hu, D. Li, J. Seaman, Y. Pan, Iodate in calcite and vaterite: Insights from synchrotron X-ray absorption spectroscopy and first-principles calculations, Geochimica Et Cosmochimica Acta, 198 (2017) 218-228.
[31] S. Wu, F. Chen, A. Simonetti, T.E. Albrecht-Schmitt, Substitution of IO3-, IO4-, SeO32-, and SeO42- for CO32- in Na-4 UO2(CO3)(3), Radiochimica Acta, 101 (2013) 625-630.
[32] X. Feng, S.A.T. Redfern, Iodate in calcite, aragonite and vaterite $CaCO_3$: Insights from first-principles calculations and implications for the I/Ca geochemical proxy, Geochimica et Cosmochimica Acta in press (2018).
[33] D. Li, D.I. Kaplan, A.S. Knox, K.P. Crapse, D.P. Diprete, Aqueous Tc-99, I-129 and Cs-137 removal from contaminated groundwater and sediments using highly effective low-cost sorbents, Journal of Environmental Radioactivity, 136 (2014) 56-63.
[34] D. Li, J.C. Seaman, D.I. Kaplan, S.M. Heald, C.J. Sun, Sequestration of pertechnetate (TcO4-) from groundwater by cost-effective organoclays and granular activated carbon: Capacity and chemical speciation, Journal of Hazardous Materials, (2018).
[35] Z. Wang, R. Abraham, Method for removing mercury and arsenic from contaminated water using an intimate mixture of organoclay and element sulfur, U.S. Patent 7,910,005 B2, in, Amcol International Corporation, Hoffman Estate, IL, USA, 2011.
[36] R.N. Strom, D.S. Kaback, SRP Baseline Hydrogeologic Investigation: Aquifer Cheracterization. Groundwater Geochemistry of the Savannah River Site and Vicinity, WSRC-RP-92-450, Westinghouse Savannah River Company, Environmental Sciences Section, Aiken, SC, 1992.
[37] D. Li, D.I. Kaplan, K.A. Roberts, J.C. Seaman, Mobile Colloid Generation Induced by a Cementitious Plume: Mineral Surface-Charge Controls on Mobilization, Environmental Science & Technology, 46 (2012) 2755-2763.
[38] A.J. Kropf, J. Katsoudas, S. Chattopadhyay, T. Shibata, E.A. Lang, V.N. Zyryanov, B. Ravel, K. McIvor, K.M. Kemner, K.G. Scheckel, S.R. Bare, J. Terry, S.D. Kelly, B.A. Bunker, C.U. Segre, The new MRCAT (Sector 10) bending magnet beamline at the Advanced Photon Source, AIP Conf. Proc., (2010) 299–302.
[39] B. Ravel, M. Newville, Athena, Artemis, Hephaestus: data analysis for X-ray absorption spectroscopy using IFEFFIT, J. Synchrotron Radiat., 12 (2005) 537–541.
[40] P.M. Harris, E. Mack, F.C. Blake, The atomic arrangement in the crystal of orthorhombic iodine, Journal of the American Chemical Society', 50 (1928) 1583-1600.
[41] D.A. McKeown, I.S. Muller, I.L. Pegg, Iodine valence and local environments in borosilicate waste glasses using X-ray absorption spectroscopy, Journal of Nuclear Materials, 456 (2015) 182-191.
[42] S. Kodama, Y. Takahashi, K. Okumura, T. Uruga, Speciation of iodine in solid environmental samples by iodine K-edge XANES: Application to soils and ferromanganese oxides, Science of the Total Environment, 363 (2006) 275-284.
[43] Y.S. Shimamoto, Y. Takahashi, Y. Terada, Formation of Organic Iodine Supplied as Iodide in a Soil-Water System in Chiba, Japan, Environmental Science & Technology, 45 (2011) 2086-2092.
[44] Y.S. Shimamoto, T. Itai, Y. Takahashi, Soil column experiments for iodate and iodide using K-edge XANES and HPLC-ICP-MS, Journal of Geochemical Exploration, 107 (2010) 117-123.
[45] X. Fan, E.C. Dickey, P.C. Eklund, K.A. Williams, L. Grigorian, R. Buczko, S.T. Pantelides, S.J. Pennycook, Atomic arrangement of iodine atoms inside single-walled carbon nanotubes, Physical Review Letters, 84 (2000) 4621-4624.
[46] L. Grigorian, K.A. Williams, S. Fang, G.U. Sumanasekera, A.L. Loper, E.C. Dickey, S.J. Pennycook, P.C. Eklund, Reversible intercalation of charged iodine chains into carbon nanotube ropes, Physical Review Letters, 80 (1998) 5560-5563.
[47] W.Y. Zhou, S.S. Xie, L.F. Sun, D.S. Tang, Y.B. Li, Z.Q. Liu, L.J. Ci, X.P. Zou, G. Wang, P. Tan, X. Dong, B. Xu, B. Zhao, Raman scattering and thermogravimetric analysis of iodine-doped multiwall carbon nanotubes, Applied Physics Letters, 80 (2002) 2553-2555.

[48] U.D. Venkateswaran, E.A. Brandsen, M.E. Katakowski, A. Harutyunyan, G. Chen, A.L. Loper, P.C. Eklund, Pressure dependence of the Raman modes in iodine-doped single-walled carbon nanotube bundles, Physical Review B, 65 (2002).
[49] N. Bendiab, R. Almairac, S. Rols, R. Aznar, J.L. Sauvajol, I. Mirebeau, Structural determination of iodine localization in single-walled carbon nanotube bundles by diffraction methods, Physical Review B, 69 (2004).
[50] T. Michel, L. Alvarez, J.L. Sauvajol, R. Almairac, R. Aznar, J.L. Bantignies, O. Mathon, EXAFS investigations of iodine-doped carbon nanotubes, Physical Review B, 73 (2006).
[51] M.S. Dresselhaus, G. Dresselhaus, Intercalation compounds of graphite, Advances in Physics, 30 (1981) 139-326.
[52] S.A. Hamid, Symmetry of KIO_3 and structure of room-temperature phase, Zeitschrift Fur Kristallographie, 137 (1973) 412-421.
[53] A. Prange, B. Birzele, J. Kramer, H. Modrow, R. Chauvistre, J. Hormes, P. Kohler, Characterization of sulfur speciation in low molecular weight subunits of glutenin after reoxidation with potassium iodate and potassium bromate at different pH values using X-ray absorption near-edge structure (XANES) spectroscopy, Journal of Agricultural and Food Chemistry, 51 (2003) 7431-7438.

488 **Table 1**

489 Fit parameters to adsorption isotherms of I^- and IO_3^- on organoclays and GAC in artificial groundwater

Sorbents	Isotherms for iodide (I^-)				Isotherms for iodate (IO_3^-)			
	pH	Langmuir fits			pH	Freundlich fits		
		q_{max} (mg I/g sorbent)	K_L (L/g)	R^2		k_f (L/g)	n	R^2
OCB	12.1	21.1	0.051	0.997	12.3	0.031	0.895	0.990
OCM	8.0	27.5	0.041	0.998	7.6	0.126	1.184	0.996
GAC 830	7.9	29.9	0.034	0.995	7.5	0.056	0.961	0.984

490

491

492 **Table 2**

493 I K-edge EXAFS fitting data of GAC 830 after exposed to iodide in artificial groundwater

Samples [a]	pH	Scattering paths	Interatomic distance (Å)	Coordination number [b]	Debye–Waller factor, σ^2 (Å^2)	E_0 (eV)	R-factor	Reduced χ^2
GAC 830-48	8.18	1st I-I	2.886 ± 0.038	1	0.0066 ± 0.0031	2.3 ± 2.7	0.0281	133
		2nd I-I	3.638 ± 0.150	2	0.0322 ± 0.0156			
		3rd I-I	4.146 ± 0.232	4	0.0624 ± 0.0432			
GAC 830-50	8.33	1st I-I	2.894 ± 0.020	1	0.0063 ± 0.0014	2.9 ± 1.4	0.0102	23.0
		2nd I-I	3.673 ± 0.102	2	0.0498 ± 0.0187			
		3rd I-I	4.397 ± 0.234	4	0.0941 ± 0.0834			
Crystalline I_2 [c]	EXAFS	1st I-I	2.837 ± 0.012	1	0.0179 ± 0.0013	8.1 ± 0.7	0.0034	1.22
		2nd I-I	3.309 ± 0.029	2	0.0773 ± 0.0119			
	X-ray structure [40]	1st I-I	2.703	1				
		2nd I-I	3.538	2				
		3rd I-I	4.348	4				

[a] Amplitude was set to 1. [b] Coordination numbers were set based on X-ray structure data. [c] Raw I_2 data was provided by McKeown at Vitreous State Laboratory, The Catholic University of America [41].

494

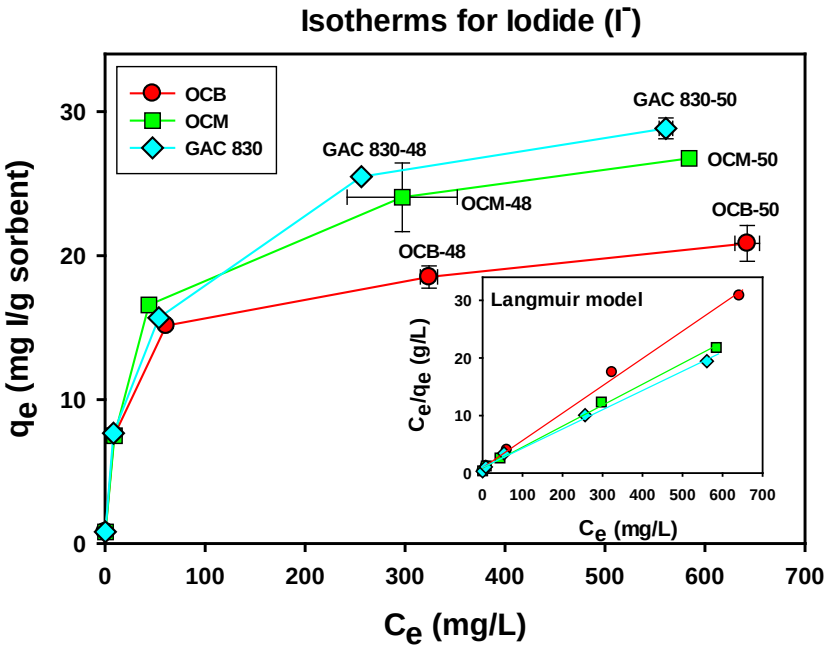

Fig. 1. Adsorption isotherms for iodide (I^-) on organoclays and GAC 830 in AGW. The isotherm data for I^- were fitted by Langmuir model (inset). The air-dried sorbent samples selected for spectroscopic measurements were labeled.

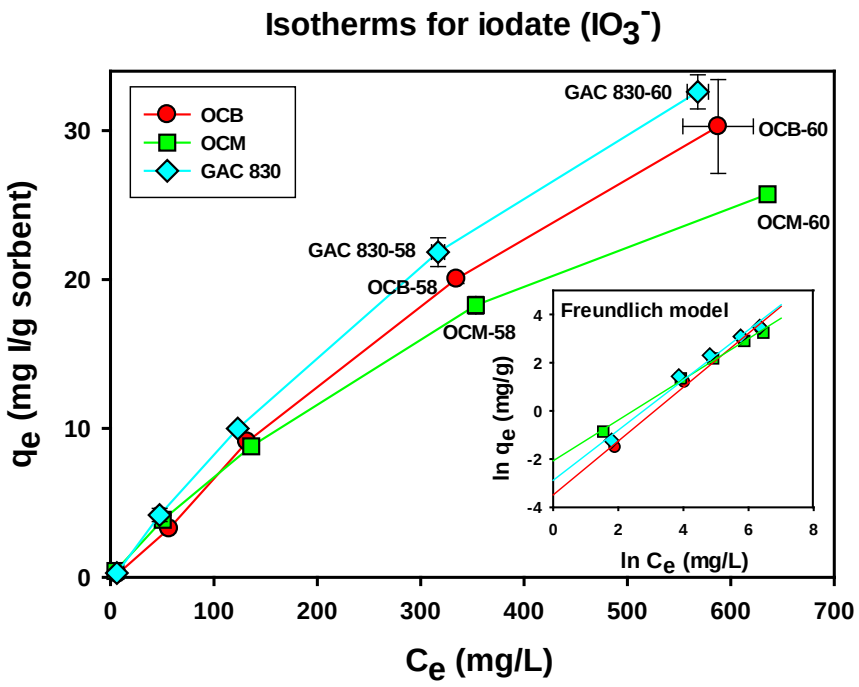

504

505 **Fig. 2.** Adsorption isotherms for iodate (IO_3^-) on organoclays and GAC 830 in AGW. The
506 isotherm data for IO_3^- were better fitted by Freundlich model (inset). The air-dried sorbent
507 samples selected for spectroscopic measurements were labeled.

508

509

510

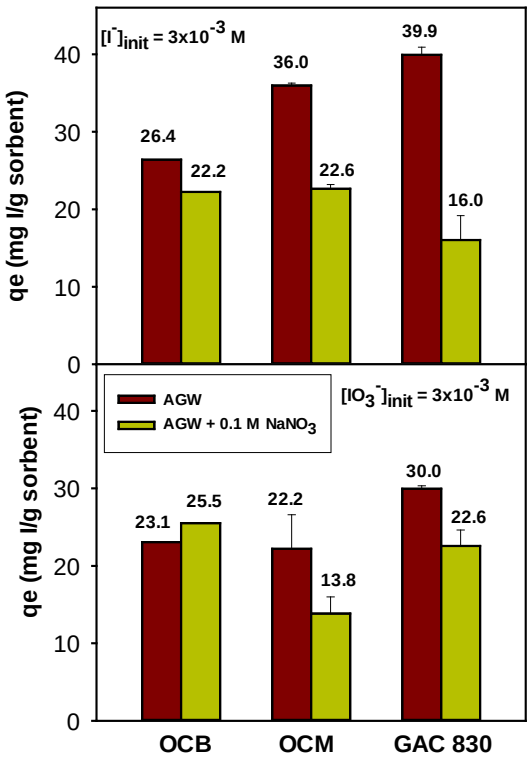

511

512 **Fig. 3.** Effects of nitrate on I^- and IO_3^- removal from artificial groundwater (AGW)

513

514

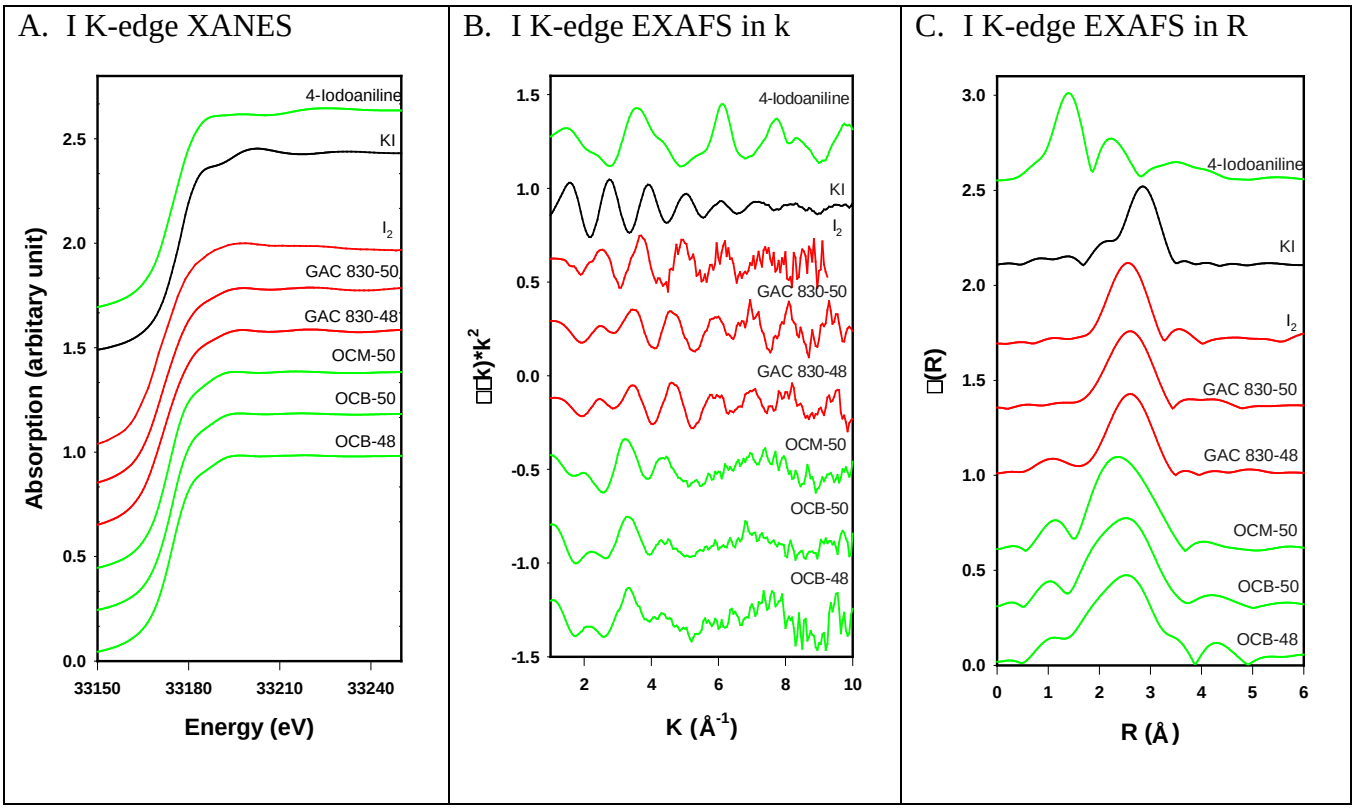

Fig. 4. I K-edge XANES (A), EXAFS spectra in k-space (B) and Fourier transform plots in magnitude (C) of organoclays (OCB and OCM) and GAC 830 after exposed to iodide (I^-) in artificial groundwater, in comparison with the corresponding spectra of I_2, KI and 4-iodoaniline.

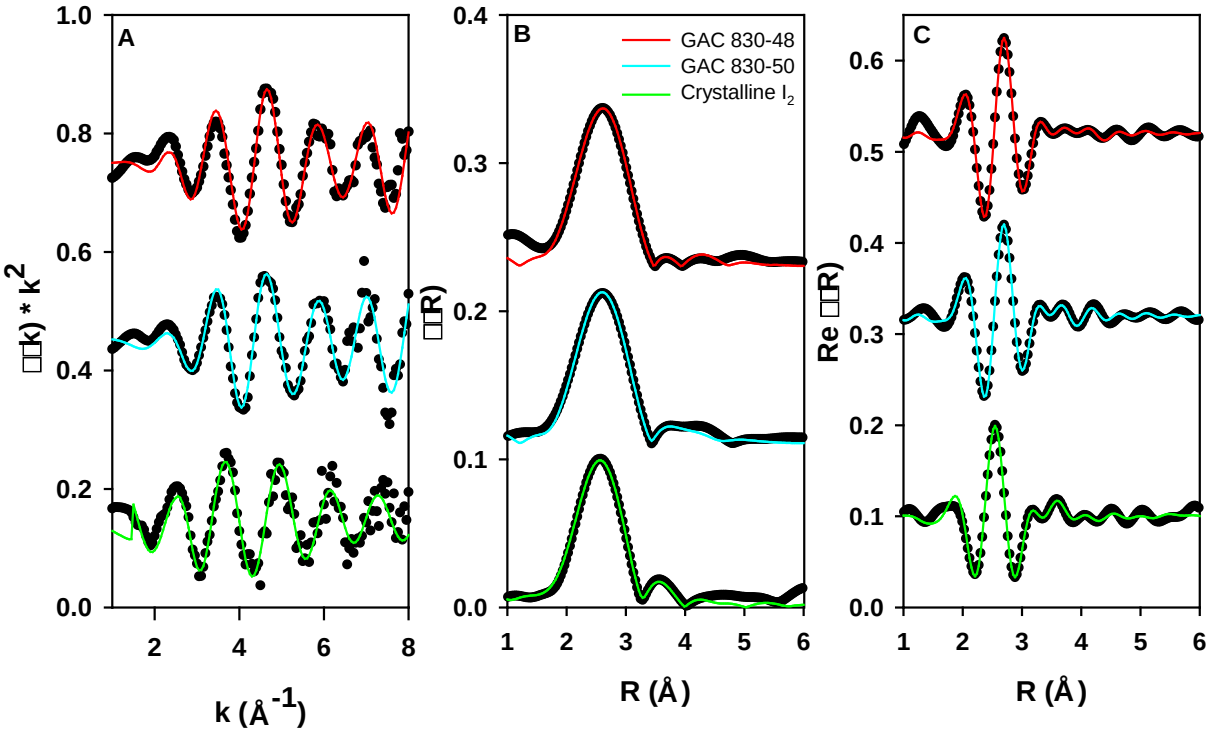

522

523

524 **Fig. 5.** I K-edge EXAFS spectra in k-space (A), Fourier transform plots in magnitude (B) and in
525 the real space component (C) of GAC 830 after exposed to iodide (I^-) in artificial groundwater
526 with the equilibrium pHs of 8.2, in comparison with the EXAFS spectra of crystalline I_2.

527

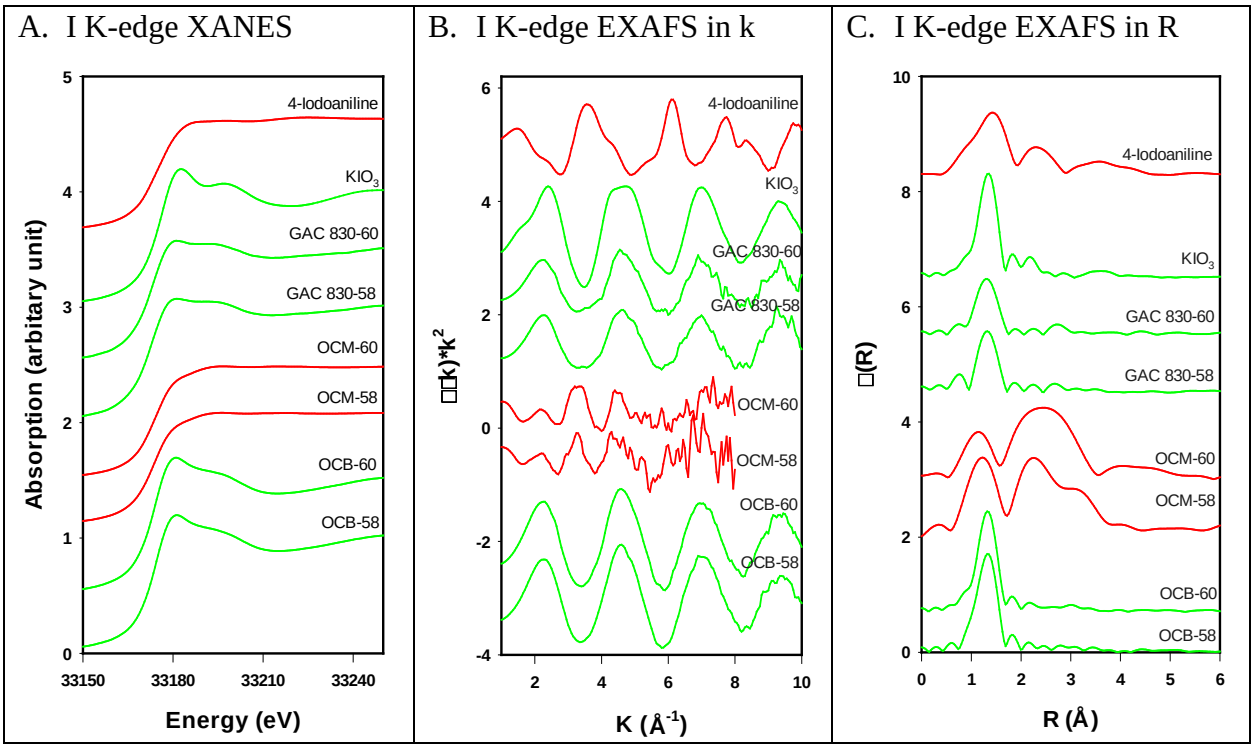

Fig. 6. I K-edge XANES (A), EXAFS spectra in k-space (B) and Fourier transform plots in magnitude (C) of organoclays (OCB and OCM) and GAC 830 after exposed to iodate (IO_3^-) in artificial groundwater, in comparison with the corresponding spectra of KIO_3 and 4-iodoaniline.